



Full Length Article

Formability, microstructure evolution and mechanical properties of wire arc additively manufactured AZ80M magnesium alloy using gas tungsten arc welding

Yangyang Guo^a, Gaofeng Quan^a, Yinglong Jiang^a, Lingbao Ren^{a,b}, Lingling Fan^a, Houhong Pan^{a,*}

^a Key Laboratory of Advanced Technologies of Materials, Ministry of Education, School of Materials Science and Engineering, Southwest Jiaotong University, Sichuan, Chengdu 610031, PR China

^b Center for Advancing Materials Performance from the Nanoscale, State Key Laboratory for Mechanical Behavior of Materials, Xi'an Jiaotong University, Xi'an 710049, PR China

Received 10 August 2019; received in revised form 9 December 2019; accepted 14 January 2020

Available online xxx

Abstract

Wire arc additive manufacturing (WAAM) technology has been used to fabricate the multi-layer single-pass deposited wall of AZ80M magnesium (Mg) alloy by gas tungsten arc welding. The formability, thermal cycles, microstructural evolution and mechanical properties of the WAAM AZ80M Mg alloy were investigated. The results show that there was significant difference in the temperature variation and the geometries between the original several layers and the subsequent deposited layers. Owing to the arc energy input, the interpass temperature rised rapidly and then stabilized at 150 °C. As a result, the width of the deposited wall increased and then kept stable. There were obvious differences in the microstructure of the WAAM AZ80M Mg alloy among the top zone, intermediate zone and bottom zone of deposited wall. During the arc deposition process, the β phase of the WAAM AZ80M Mg alloy redissolved due to the cyclic heat accumulation, and then precipitated in the grain boundary. The cyclic heat accumulation also led to weakening of dendrite segregation. From the substrate to the top zone, the hardness of the deposited wall decreased gradually, and the intermediate zone which was the main body of deposited wall had relatively uniform hardness. The tensile properties of the WAAM AZ80M Mg alloy were different between the vertical direction and the horizontal direction. And the maximum ultimate tensile strength of the WAAM AZ80M Mg alloy was 308 MPa which was close to that of the as-extruded AZ80M Mg alloy.

© 2020 Published by Elsevier B.V. on behalf of Chongqing University.

This is an open access article under the CC BY-NC-ND license. (<http://creativecommons.org/licenses/by-nc-nd/4.0/>)

Peer review under responsibility of Chongqing University

Keywords: Wire arc additive manufacturing; Magnesium alloy; Thermal cycles; Microstructure; Mechanical properties.

1. Introduction

Magnesium (Mg) has attracted great attention in recent years because of its excellent properties, such as high specific strength, good damping, electromagnetic shielding, machining, recyclability and biodegradability, etc. [1,2]. Mg alloys are preferred when targeting weight-sensitive applications, and play an important role in lightweighting and energy

saving and emission reduction [3,4]. With the further development of lightweight technology and the further application of Mg alloys, design and manufacture of Mg alloys parts with high quality and complex shape is an urgent request in the automobile, aerospace, and railway transportation industry [5]. The parts of Mg alloys are usually fabricated by traditional manufacturing methods, such as deformation processing and casting. However, deformation processing always needs to be performed at elevated forming temperatures due to the poor cold workability of Mg alloys, which leads to the oxidation of the parts and the limited efficiency [6]. Casting used to

* Corresponding author.

E-mail address: houhongpan@home.swjtu.edu.cn (H. Pan).

<https://doi.org/10.1016/j.jma.2020.01.003>

2213-9567/© 2020 Published by Elsevier B.V. on behalf of Chongqing University. This is an open access article under the CC BY-NC-ND license. (<http://creativecommons.org/licenses/by-nc-nd/4.0/>) Peer review under responsibility of Chongqing University

ensure great efficiency with higher precision, but the mechanical properties are degraded because of the coarse grain and the slag inclusion of oxides [7,8]. Thus, new manufacturing methods are desired to produce monolithic parts of Mg alloys.

Wire arc additive manufacturing (WAAM), as a kind of additive manufacturing (AM) technologies, offers a promising alternative to traditional subtractive manufacturing of metallic parts. To fabricate parts or components, metal wire is fed at a constant speed and is melted by arc onto a substrate or the previous deposited layers [9]. Compared with the powder-based additive manufacturing technique or wire-feed AM using laser or electron beam as heat source, WAAM exhibits a higher deposition rate, better material utilization efficiency and energy saving effect, which reveals a great potential to fabricate the large structures using poor deformable metallic materials [10-12]. WAAM has been applied to the net-shape processing of various metallic materials, such as titanium alloys [13-15], steel [16,17], aluminum alloys [18-20], etc.

It is generally accepted that the microstructure and mechanical properties of the as-deposited parts depend on its thermal history during the WAAM process. As the welding arc moving, the part is built layer by layer, and the formed layers experience a cycle of heating and cooling. Due to the multiple fusion, solidification, and phase transformation, the heat dissipation is highly non-linear [21-23]. Heat accumulation has been reported as a critical factor which influences the microstructural evolution, deposition defects, geometrical accuracy, and mechanical properties [24]. Wang et al. [25] reported that during the arc-wire deposition process, the distance between the trailing end and the center of molten pool was increased by 1.95 mm from 1st layer to 5th layer due to the increase of heat accumulation. Ma et al. [26] investigated the fabrication of Ti-Al alloy part using Gas Tungsten-WAAM (GT-WAAM) and found that the fraction of α -phase in the microstructure decreased by nearly threefold when the interpass temperature increased from 100°C to 400°C, which resulted in the decrease of hardness. Up to present, studies focused on WAAM of Mg alloys have rarely been reported. Guo et al. [5] preliminarily applied WAAM to fabricate AZ31 Mg alloy, and the results revealed that the ultimate tensile strength (UTS) and yield strength (YS) of the WAAM AZ31 were similar to those of the forged ones. Hisataka et al. [27] evaluated the properties of the WAAM Mg alloys based on adjusting the process parameters, in which the fabricated object possessed the sufficient tensile strength compared to the standard value of the bulk Mg alloys. In the present study, a 50-layers deposited wall of AZ80M Mg alloy was fabricated based on GT-WAAM and the forming characteristics, thermal cycle, microstructural evolution and mechanical properties were investigated and discussed.

2. Materials and experimental procedures

The nominal chemical composition of the AZ80M Mg alloy was Mg-8.5Al-0.45Zn-0.03Mn-0.15Ca-0.2Y, wt%. Adding 0.2 wt% Y (Yttrium) can markedly improve the strength and ductility of Mg alloys [28]. The 1.6 mm diam-

Table 1
Processing parameters for the GT-WAAM deposition.

Processing parameters	Variable	Value
Deposition power	Peak current	120 A
	Base current	75 A
	Frequency	8 Hz
Speed	Travel speed	300 mm/min
	Wire feeding speed	1150 mm/min
Distance and angle	Electrode to workpiece (distance)	5 mm
	Electrode to filler wire (angle)	30°
	Flow rate (argon)	GTAW torch
Time	Dwell time between layers	160 s

eter of AZ80M wire and the 8 mm × 80 mm × 150 mm sizes of AZ80M extrusion plate were employed in the GT-WAAM process. The surface of the substrate plate was polished and then cleaned by acetone before the deposition.

50-layers single-pass AZ80M deposited wall was fabricated. The processing parameters are presented in Table 1, and three workpieces were prepared under the same parameters. Before deposition, the substrate was at room temperature. The shielding gas used for this work was 99.99% Ar, which was helpful to avoid the oxidation and the contaminants of the molten pool. A schematic diagram of the GT-WAAM system is displayed in Fig. 1. The wire was fed in front of the molten pool and the angle between the wire feeding nozzle and the substrate surface was 30° 5 mm of distance was kept between the electrode and the workpiece, which allowed smooth wire fed to the molten pool and kept the stability of the arc voltage. During the deposition process, the substrate plate was kept fixing, and the welding torch moved along the deposition direction.

The preparation of samples is shown in Fig. 2. In order to measure the temperature of the deposition process in real time, a thermocouple was fixed 2 mm below of the substrate surface (see Fig. 2b) for continuously monitoring the substrate temperature. The cross-section samples were cut from the deposited wall by wire electrical discharge machining. And these samples were grounded by SiC abrasive papers to 2000 grit, polished to a mirror-like finish, etched using a solution of 4.2 g picric acid, 10 ml acetic acid, 10 ml distilled water and 100 ml alcohol. The microstructure and the element distribution at the different regions of the deposited wall were analysed by optical microscopy (Zeiss Lab. A1 optical microscope), scanning electron microscopy (SEM) and energy dispersive X-ray spectroscopy (EDS) (SEM, Quanta FEG 250 equipped with an EDS analysis system). The phase composition was analyzed by Panalytical X'Pert Pro-with the angle ranges from 20° to 80° Hardness profile along the deposition direction was measured with a load of 25 gf and a dwell time of 15 s using HXD-1000TM Vickers hardness tester. Tensile properties were measured in both the horizontal and vertical directions. Fig. 2c and d shows the dimensions for the tensile specimens at the horizontal and vertical directions,

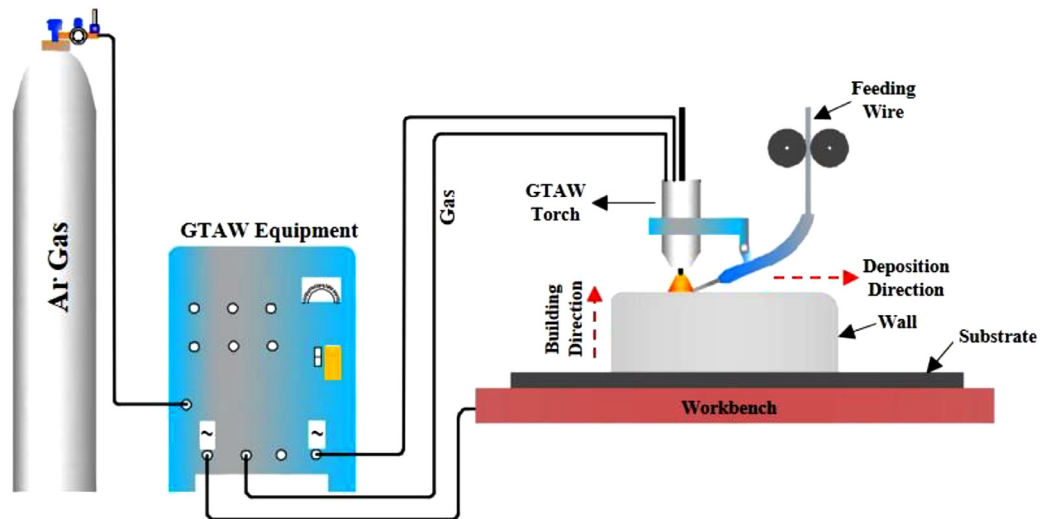


Fig. 1. Schematic map of the experimental setup for GT-WAAM.

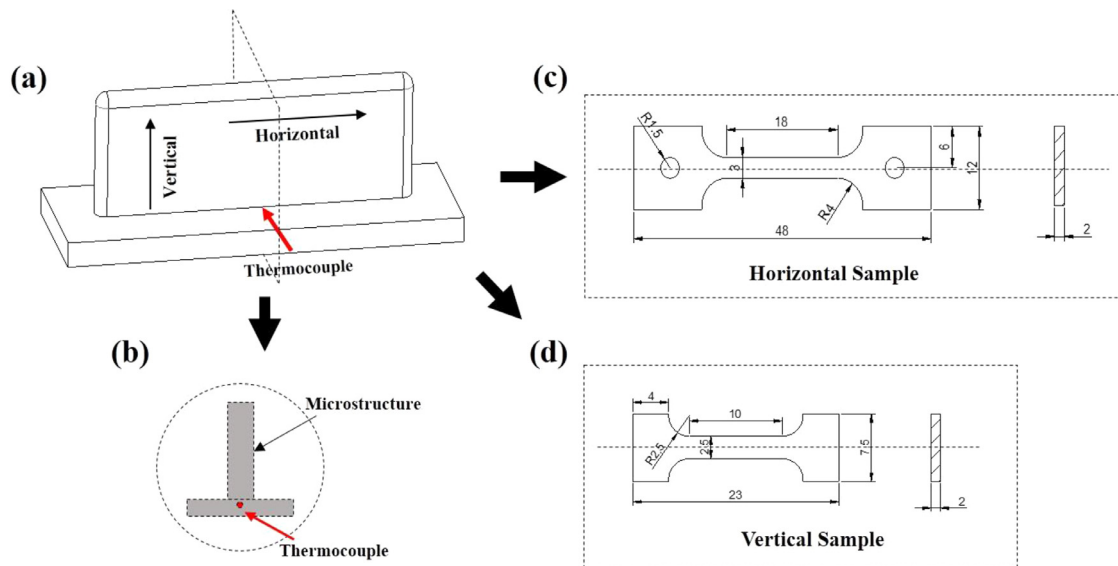


Fig. 2. Sample preparation: (a) direction definition of the WAAM deposited wall structure, (b) the cross-section for microstructure observations, dimensions of the (c) horizontal tensile specimen and (d) the vertical tensile specimen.

respectively. The tensile test was carried on the MTS-CMT5105 universal testing machine at room temperature with a cross-head speed of 0.5 mm/min.

3. Results and discussion

3.1. Geometrical features and thermal monitoring

Fig. 3 shows the width of the cross section of the WAAM AZ80M deposited wall along the building direction. It can be divided into two zone: unstable and stable zone. The width of the unstable zone consisting of the 1st to the 6th layer increased from 9 mm to 11 mm, while the width of the stable zone kept at about 11–12 mm. It is widely accepted that the welding bead was solidified from the molten pool, and the morphology of the molten pool was related to the temperature

of the substrate [29]. As the substrate was at room temperature in the initial stage of the depositing process, greater temperature gradient generated between the molten pool and the substrate, and the heat of the molten pool was readily lost through the substrate. Meanwhile, Mg alloys had very good thermal conductivity [30], which also exacerbated the heat dissipation of the molten pool. As a result, the size of the molten pool was smaller. Correspondingly, the width of the deposited layer was narrower. With the deposition proceeding, the thermal resistance coefficient increased with the increase of the temperature of the substrate and the deposited layer, which decreased the heat dissipation of the molten pool and resulted in the increase of the size of the molten pool and the width of the deposited layer. When the balance between heat input and heat dissipation of the molten pool was established, the width of the deposited layer tended to be stable. However,

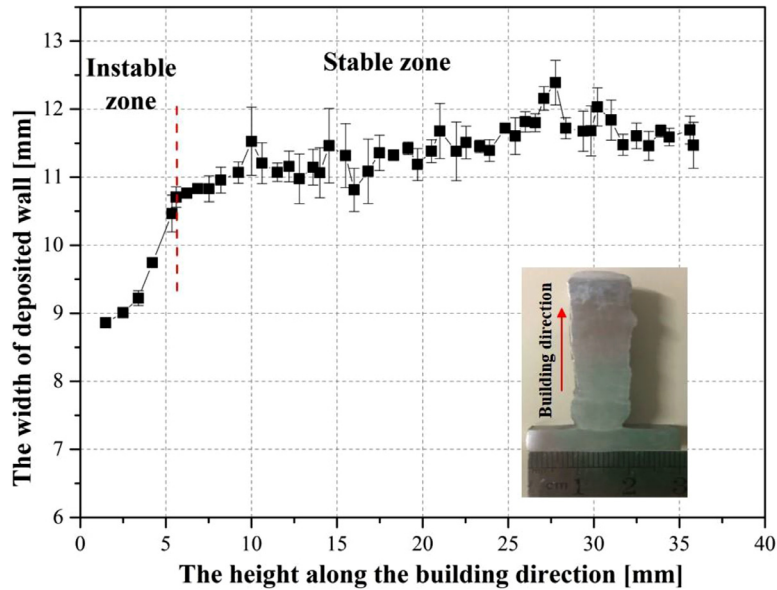


Fig. 3. Width of the cross-section of the deposited wall along the building direction.

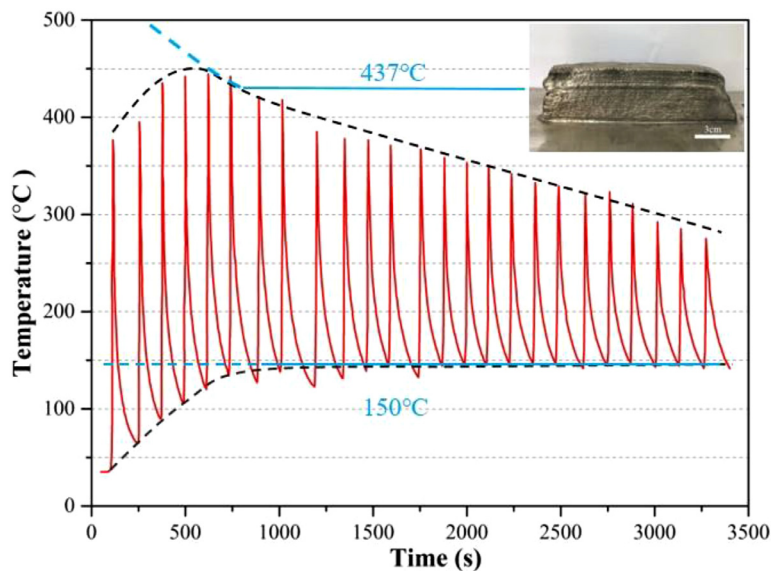


Fig. 4. Temperature variation with time during the WAAM process.

a slight rise in the curve can still be found in the stable zone, which was mainly caused by the shape-change of electrodes tip. The gradual transformation of tungsten pole from conical to spherical led to the arc radiate and increased the width of the deposited layer [31].

Fig. 4 shows the thermal cycles of the substrate measured by thermocouple (as presented in Fig. 2b) during the deposition process. It can be seen from Fig. 4 that the curve was composed of a series of peaks and troughs. The peak temperature increased in the first several deposition process and then decreased gradually with the process proceeding, while the trough temperature continually climbed up in the first several deposition process and then kept stable at 150 °C. Since the temperature of the substrate was initially at room temperature and the substrate had best heat conduction condition,

this resulted in the low peak and trough temperatures at the first several layers. With the subsequent depositions proceed, the heat accumulation of the substrate increased gradually. Therefore, the increases of both peak and trough temperatures can be observed in the first several cycle. Under the same conditions, the closer the distance from the thermocouple is, the higher the temperature measured is. As the deposition proceeded, the distance between the heat source and the temperature measurement point increased. Therefore, the peak temperature decreased gradually. At the same time, the establishment of the balance between the heat input and the heat dissipation kept the trough temperature stable. The temperature was regarded as a key factor for investigating the thermal behavior of the AM processes by some researchers [24,32-34]. During arc-based deposition process, previous

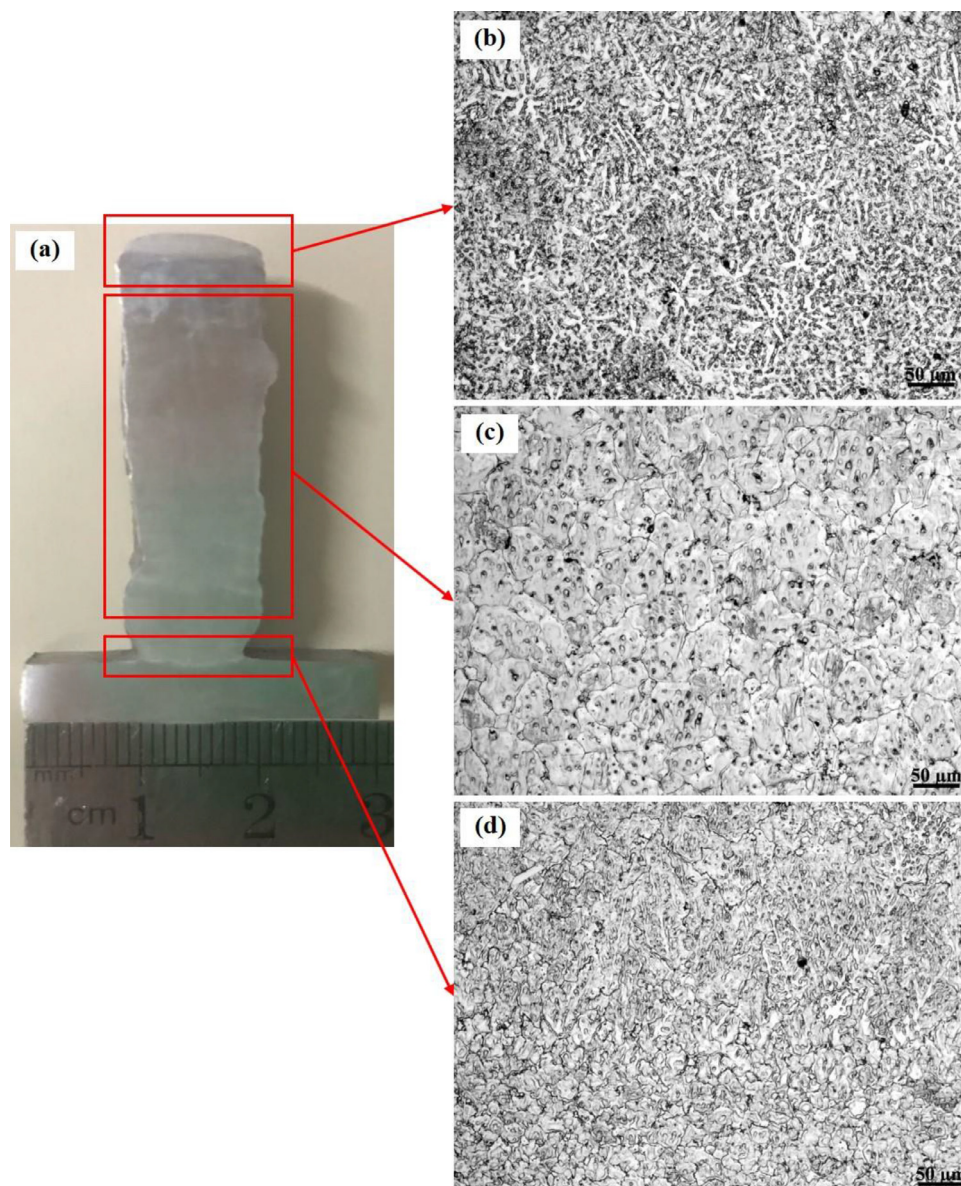


Fig. 5. Microstructure of the WAAM AZ80M deposited wall in the cross-section. (a) Overall image, (b) the top zone, (c) the intermediate zone, (d) the bottom zone.

deposited layers underwent a complicated thermal history (including rapidly heating, melting, cooling, solidification, and even partial remelting) and a repeated thermal cycling [34]. As shown in Fig. 4, though the temperature of the substrate increases gradually from room temperature during the deposition of the initial layers, the electric arc with high energy density could heat the previous deposited layer near or more than 437 °C (the eutectic temperature of Mg-Al) during the subsequent several depositions, and the whole deposited wall would be kept at the trough temperature of 150 °C for a long time. It would make a great influence on the structure of deposited wall [35]. If the thermocouple is installed under the newly deposited layer in the intermediate zone of the deposited wall, the peak temperature and the trough temperature of subsequent thermal cycles will vary as shown by the blue dot line in Fig. 4.

3.2. Microstructure evolution of the AZ80M deposited part

Fig. 5 shows the microstructures of the different regions on the cross-section of the WAAM AZ80M deposited wall. As shown in Fig. 5a, no obvious defects, like cracks, pores and incomplete fusion were found in the deposited wall or the interface between the deposited metal and the substrate. It can also be seen from Fig. 5 that the microstructures of the different regions were quite different [36]. Fig. 5b reveals that the top zone of the deposited wall was composed of a large number of equiaxed and dendritic crystals which were the typical welding microstructure. In the meantime, an obvious dendrite segregation can be seen in this zone. The microstructure of the intermediate zone (Fig. 5c) which represented the most part of the deposited wall was still equiaxed crystal, but the dendrite segregation in the intermediate zone

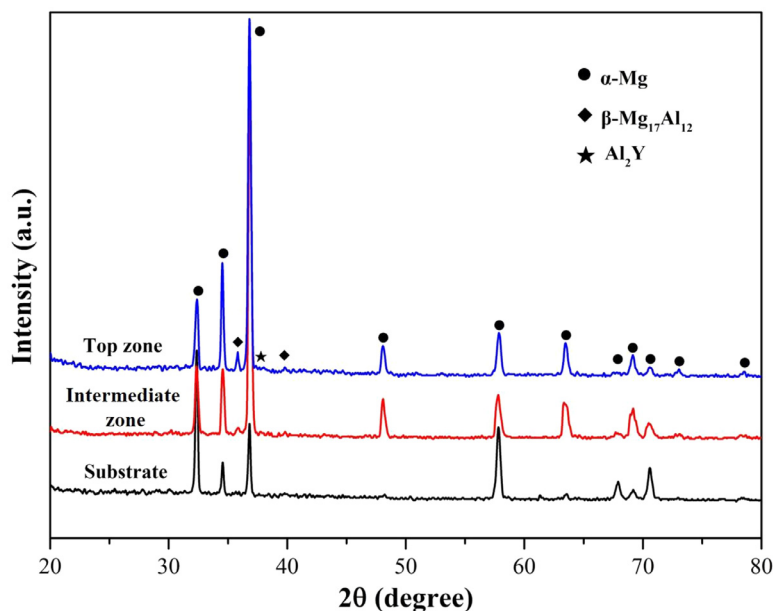


Fig. 6. The X-ray diffraction spectra for the top zone, intermediate zone and substrate.

was less than that in the top zone. Fig. 5d reveals a typical columnar dendritic grain in the bottom zone of the deposited wall. The reason was that there was a large temperature gradient between the molten pool and the substrate, which led to an epitaxial growth of the columnar grain along the fusion line and gradually evolved into a larger size of columnar dendritic grain. XRD patterns (Fig. 6) indicated that there were a series similar positions of peaks in the top zone and the intermediate zone. And the phase composition consisted of α -Mg, β -Mg₁₇Al₁₂ and a small amount of Al₂Y [36,37].

In order to better understand the evolution of microstructures during deposition, SEM was used to observe the microstructures of the 50th (top layer)–46th layers in the top zone and the 25th layer in the intermediate zone of the WAAM AZ80M deposited wall. As shown in Fig. 7a–e, along the deposited direction, the variation of the microstructure of the 50th–46th layers was obvious. From the 50th layer to the 46th layer, the proportion of the second phase, i.e. the bright white phase, was 7.95%, 6.72%, 6.35%, 4.56% and 3.75%, respectively. The phenomenon of the dendrite segregation was clearly weakened, and the bulk divorced eutectic phase along the grain was gradually dissolved in the matrix or partly transformed into a fine granular dispersion distribution. On the contrary, the proportion of the white second phase significantly increased to 6.51% in the 25th layer (Fig. 7f). The transition characteristics of the 50th layer and the 25th are revealed at higher magnification in Fig. 8a and b. As Fig. 8a showed, in the layer 50, the most of β phase was coarse strip which was distributed in the grain boundary, while a small amount was granular which was distributed in α -Mg. The results of the EDS analysis indicated that the bright white phase (Fig. 8c) was Mg–Al divorced eutectic (α -Mg and β -Mg₁₇Al₁₂) (arrow A: Mg_{73.60}Al_{24.57}Zn_{0.57}Ca_{1.26}) and the dark gray phase (Fig. 8d) was α -Mg matrix (arrow

B: Mg_{96.65}Al_{3.35}). In Fig. 8b, the layer 25 revealed that the fine short bar β phase and the granular β phase (Fig. 8e) were discontinuously precipitated in the grain boundary (arrow C: Mg_{64.68}Al_{35.32}). The effect of the heat accumulation of subsequent deposition process on the microstructure of the previous deposited layers was critical [24,36]. Based on the heat flow diagram (Fig. 4), the deposited layer underwent an instantaneous peak temperature of 400–450 °C during the subsequent several depositions, which approaching or exceeding the eutectic temperature of Mg–Al alloy (437 °C). Therefore, the second phase in the deposited layer was partially redissolved. After that, the deposited layer kept at 150 °C for a long time, which promoted the discontinuous precipitation of the second phase [35].

3.3. Mechanical properties of the AZ80M deposited part

The hardness distribution of the WAAM AZ80M deposited wall is shown in Fig. 9. From the substrate to the top zone, the hardness was different, ranging from 84 HV to 68 HV. The hardness distribution was in accordance with the microstructural observation and the microchemical distribution measurements. The hardness of the substrate had the highest value of 84 HV. The decrease of the hardness can be observed in the bottom region, which was induced by the gradual coarsening of the grains (Fig. 5d) and the change of the composition due to the different dilution rate of base metal. Although the hardness of the intermediate zone fluctuated slightly due to the uneven distribution of interlaminar grains, it was relatively uniform because of the dissolution and the re-precipitation of the second phase under the effect of cyclic heat, with a mean hardness value of 74 HV. Compared with the hardness of the intermediate zone, the hardness value of 72 HV in the top zone was lower and the fluctuation was more obvious

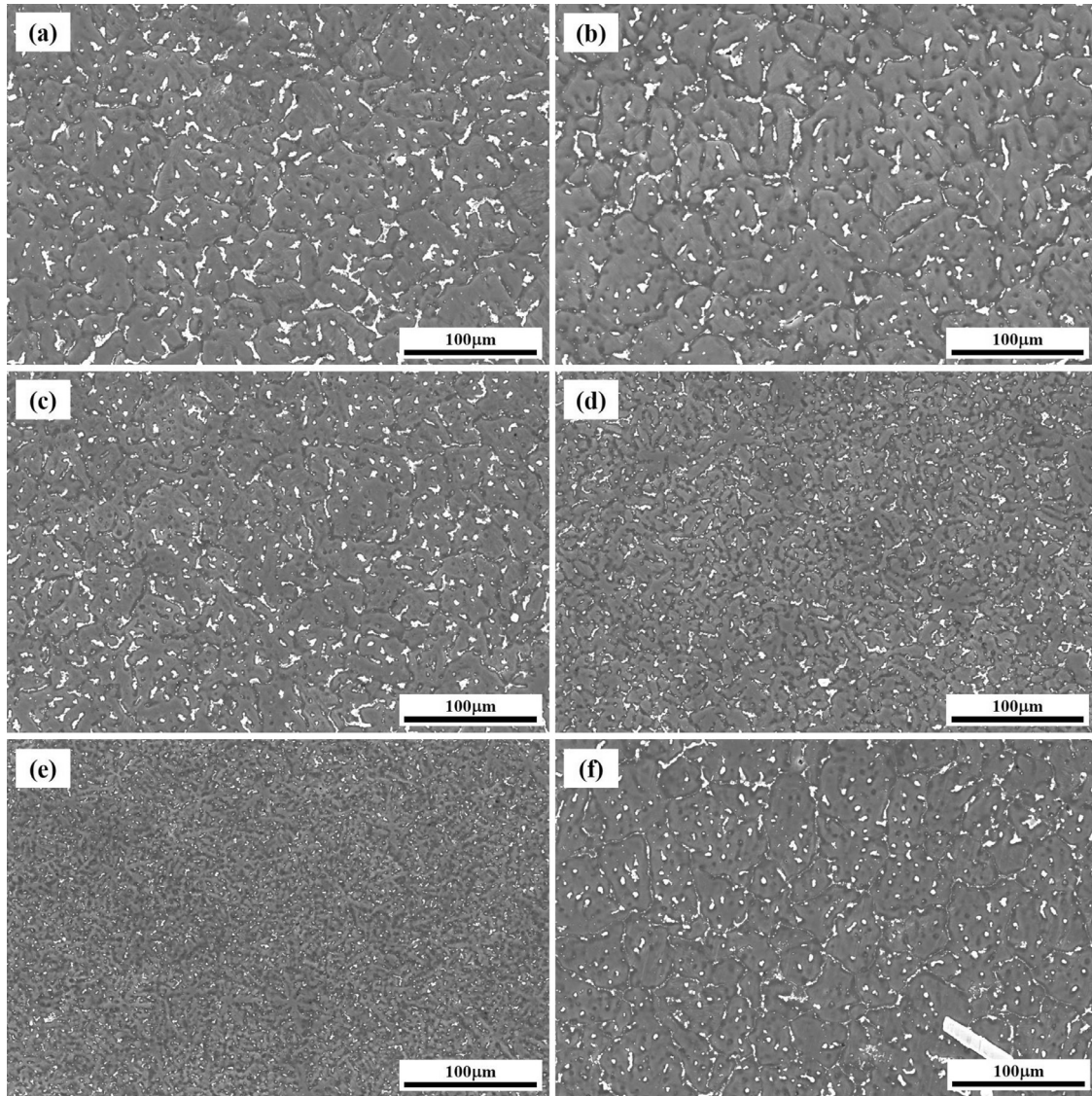


Fig. 7. SEM images of the microstructures of the WAAM AZ80M deposited wall at the different layers: (a-e)50th-46th layers, (f) 25th layer.

because of non-equilibrium solidified structure with obvious segregation.

The inhomogeneity of the microstructure of WAAM AZ80M deposited wall along the deposition direction may lead to the anisotropy of the tensile properties. Therefore, the tensile tests in horizontal and vertical directions (set as the WAAM AZ80M D-H and the WAAM AZ80M D-V) were carried out and the test results are shown in Fig. 10 and Table 2. YS, UTS and elongation (EL) of the WAAM AZ80M D-H samples were 146 MPa, 309 MPa and 15%, respectively. YS, UTS and EL of the WAAM AZ80M D-V samples were 119 MPa, 237 MPa, and 12%, respectively. YS, UTS and EL of the WAAM AZ80M D-H samples was higher than that of the WAAM AZ80M D-V samples. As a contrast, as-cast AZ80M and as extruded (ED: extruded direction) AZ80M were also tested. The as-extruded AZ80M had the best tensile properties with its YS, UTS, and EL of 207 MPa, 324 MPa and 17%, respectively. Moreover, the as-cast AZ80M revealed

Table 2

Tensile properties of AZ80M Mg alloy under the different processing conditions.

Processing conditions	YS (MPa)	UTS (MPa)	EL (%)
As-cast	76 ± 61.7	158 ± 2.9	7 ± 0.2
WAAM D-V	119 ± 13.4	237 ± 6.3	12 ± 0.7
WAAM D-H	146 ± 46.7	308 ± 6.5	15 ± 0.5
As-extruded	207 ± 4.5	324 ± 2.5	17 ± 0.6

a worst tensile performance with its YS, UTS, and EL of 76 MPa, 158 MPa and 7%, respectively. The asymmetry performances in the direction of D-V and D-H are considered to be related to the deposition process and the microstructures. During the next deposition process, the upper metal of the previous deposited layer was remelted into the molten pool, mixed with the fed wire to form a new molten pool, and then solidified. The interface zone between the newly

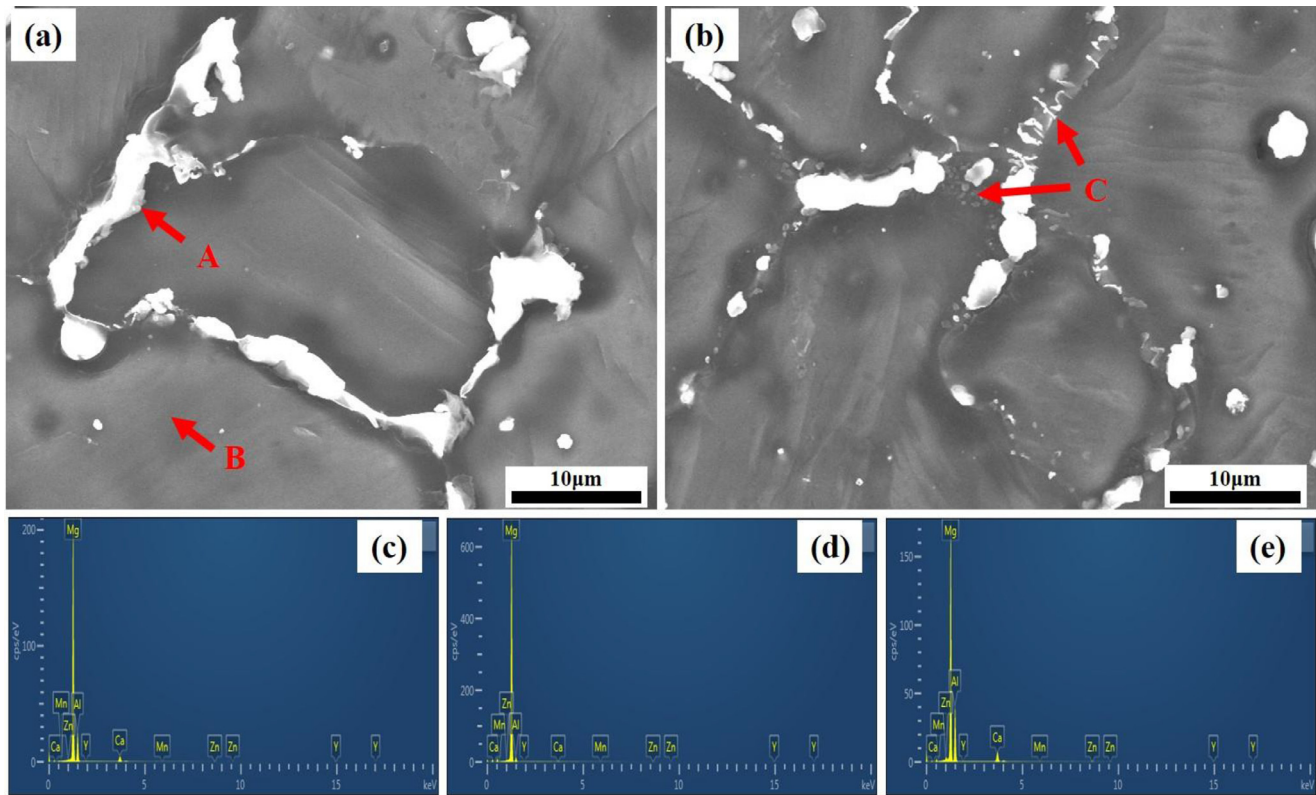


Fig. 8. The zoomed-in SEM images at the different layers: (a) 50th layer, (b) 25th layer; and the EDS spectra of phases for: (c) arrow A; (d) arrow B and (e) arrow C.

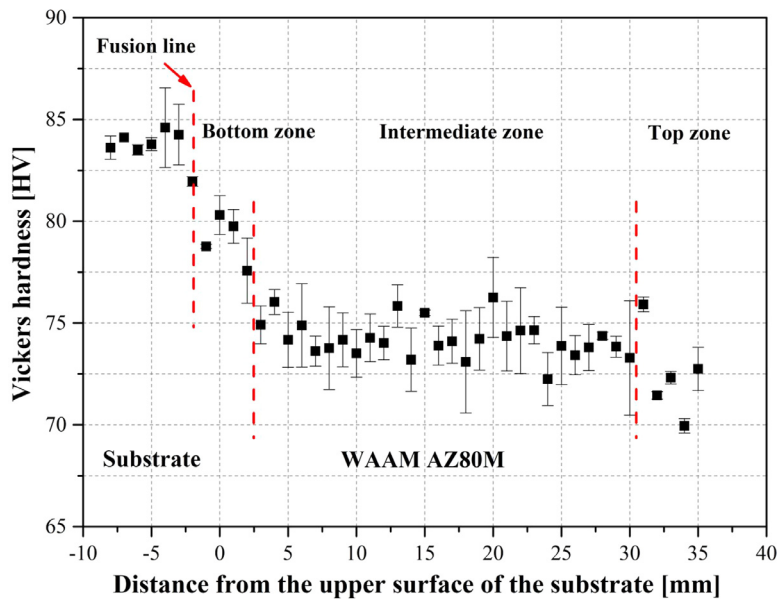


Fig. 9. Hardness distribution of the WAAM AZ80M deposited wall along the building direction.

built deposited layer and the previous deposited layer was not only the interface between the two layers, but also the solid-liquid boundary during the solidification process. In the interface zone, the heating process as well as the distribution of grains were complex. Usually, coarse grains, a large number of micro pores and micro cracks were produced in

this zone, which reduced the tensile properties of the specimen in the D-V direction and caused the asymmetry of the mechanical properties in the horizontal and vertical direction. This phenomenon has been reported by Zhang et al. [11], Lu et al. [17] and our previous research [36]. It can be concluded that the tensile properties of AZ80M Mg alloy with

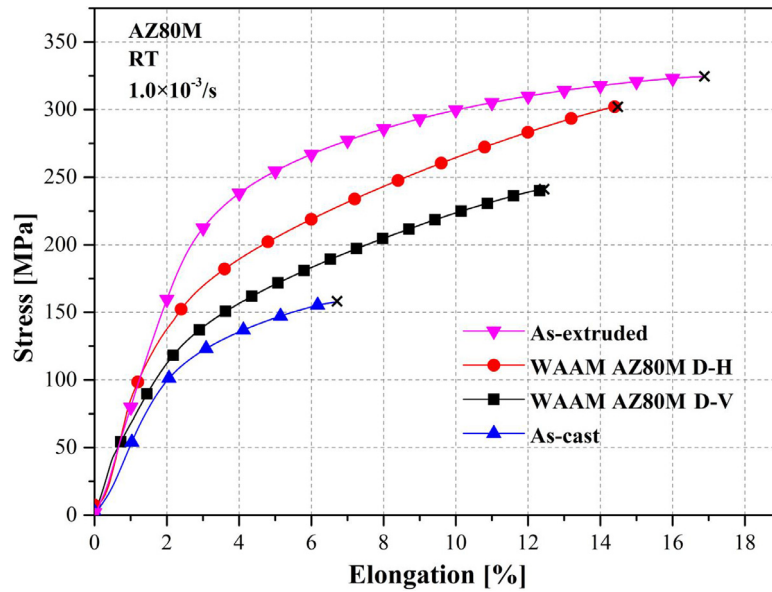


Fig. 10. Tensile curves for the AZ80M Mg alloy under the different processing conditions.

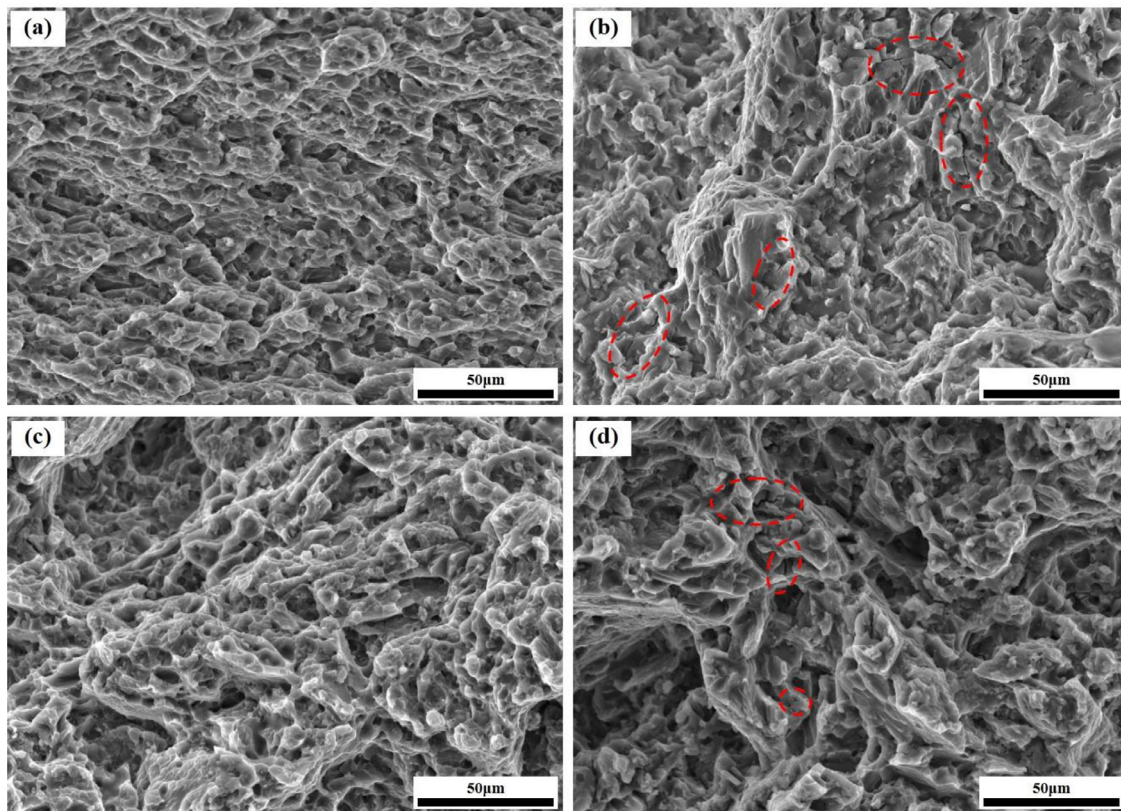


Fig. 11. Fracture morphology of AZ80M Mg alloy under the different processing conditions. (a) as-extruded, (b) as-cast, (c) WAAM D-H, (d) WAAM D-V.

a decreased performance was in this sequence: as-extruded AZ80M, WAAM AZ80M D-H, WAAM AZ80M D-V, as-cast AZ80M.

SEM images of the tensile fracture surface of AZ80M under the different processing conditions are shown in Fig. 11. The fracture surface of the as-extruded AZ80M mainly exhibited the feature of a ductile fracture, which was characterized

by more dimples and tearing ridges (Fig. 11a). By contrast, cleavage surfaces, secondary cracks (marked with red dotted circle in Fig. 11b), and secondary-phase particles, which were taken as typical brittle fracture features, could be seen on the fracture surface of the as-cast AZ80M. The number of dimples on the fracture surface of the WAAM AZ80M D-H (Fig. 11c) was significantly higher than that on the fracture

surface of the WAAM AZ80M D-V, and the size of the second phase particles was more refinement and uniform distribution. Meanwhile, obvious secondary cracks were observed on the fracture surface of the WAAM AZ80M D-V (marked with red dotted circle in Fig. 11d). The microstructure near the fracture location revealed that it was more uniform in the WAAM AZ80M D-H samples than that in the WAAM AZ80M D-V samples. In addition, there were usually a large number of interlaminar micro-cracks or micro-pore defects in the interlayer positions [38], which were formed under the tensile force. The stress concentration eventually formed cracks and caused fracture.

4. Conclusion

In this study, AZ80M Mg alloy has been used as the build material for GT-WAAM process to fabricate a thin wall. The influence of heat evolution and the thermal cycle feature on the wall geometry, the microstructure transition, and the mechanical properties were investigated. The main conclusions are drawn as follows:

1. The interpass temperature had an important influence on the width of deposited layer. Owing to the influence of heat accumulation, the temperature of the substrate rised rapidly and then stabilized at 150 °C, and the bead width increased and then kept stable synchronously.
2. The main reason for the obviously inhomogeneous characteristics was that the arc thermal cycle makes the workpiece undergo a complex variable amplitude thermal cycle. The divorced eutectic phase first dissolves into the magnesium matrix, and then precipitated on the grain boundary as β phase.
3. The hardness distribution along the deposition direction is uneven, and the average hardness of the middle is 74HV. The maximum UTS of the WAAM AZ80M was 308MPa which was close to that of the as-extruded AZ80M and much higher than as-casted AZ80M.

Acknowledgment

This work was supported by the China Scholarship Council (No. 201907000039), the national key research and development plan of China (grant number 2017YFB0305905) and the Doctoral Innovation Fund Program of Southwest Jiaotong University (No. D-CX201830).

References

- [1] B.L. Mordike, T. Ebert, *Mater. Sci. Eng. A* 302 (2001) 37–45.
- [2] M.K. Kulekci, *Int. J. Adv. Manuf. Technol.* 39 (2008) 851–865.
- [3] A. Kumar, S. Kumar, N.K. Mukhopadhyay, *J. Magn. Alloy* 6 (2018) 245–254.
- [4] L.B. Ren, L.L. Fan, M.Y. Zhou, Y.Y. Guo, Y.W.X. Zhang, C.J. Boehlert, G.F. Quan, *Int. J. Lightweight Mater. Manuf.* 1 (2018) 81–88.
- [5] J. Guo, Y. Zhou, C.M. Liu, Q.R. Wu, X.P. Chen, J.P. Lu, *Materials (Basel)* 9 (2016) 823–831.
- [6] R. Gehrman, M.M. Frommert, G. Gottstein, *Mater. Sci. Eng. A* 395 (2005) 338–349.
- [7] K.W. Wei, M. Gao, Z.M. Wang, X.Y. Zeng, *Mater. Sci. Eng. A* 611 (2014) 212–222.
- [8] K.W. Wei, Z.M. Wang, X.Y. Zeng, *Mater. Lett.* 156 (2015) 187–190.
- [9] S.W. Williams, F. Martina, A.C. Addison, J. Ding, G. Pardal, P. Colegrove, *Mater. Sci. Technol.* 32 (2016) 641–647.
- [10] F.D. Wang, S. Williams, P. Colegrove, A.A. Antonysamy, *Metall. Mater. Trans. A* 44 (2012) 968–977.
- [11] C. Zhang, Y.F. Li, M. Gao, X.Y. Zeng, *Mater. Sci. Eng. A* 711 (2018) 415–423.
- [12] D.H. Ding, Z.X. Pan, D. Cuiuri, H.J. Li, *Int. J. Adv. Manuf. Technol.* 81 (2015) 465–481.
- [13] J.K. Zhang, X.Y. Wang, S. Paddea, X. Zhang, *Mater. Des.* 90 (2016) 551–561.
- [14] J.J. Lin, Y.H. Lv, Y.X. Liu, B.S. Xu, Z. Sun, Z.G. Li, Y.X. Wu, *Mater. Des.* 102 (2016) 30–40.
- [15] M.J. Bermingham, D. Kent, H. Zhan, D.H. StJohn, M.S. Dargusch, *Acta Mater* 91 (2015) 289–303.
- [16] X.H. Chen, J. Li, X. Cheng, B. He, H.M. Wang, Z. Huang, *Mater. Sci. Eng. A* 703 (2017) 567–577.
- [17] X. Lu, Y.F. Zhou, X.L. Xing, L.Y. Shao, Q.X. Yang, S.Y. Gao, *Int. J. Adv. Manuf. Technol.* 93 (2017) 2145–2154.
- [18] J.L. Gu, X.S. Wang, J. Bai, J.L. Ding, S. Williams, Y.C. Zhai, K. Liu, *Mater. Sci. Eng. A* 712 (2018) 292–301.
- [19] Z.W. Qi, B.Q. Cong, B.J. Qi, G. Zhao, J.L. Ding, *Mater. Lett.* 230 (2018) 275–278.
- [20] J.H. Ouyang, H. Wang, R. Kovacevic, *Mater. Manuf. Process.* 17 (2002) 103–124.
- [21] L. Thijs, F. Verhaeghe, T. Craeghs, J.V. Humbeeck, J.P. Kruth, *Acta Mater.* 58 (2010) 3303–3312.
- [22] D. Herzog, V. Seyda, E. Wycisk, C. Emmelmann, *Acta Mater.* 117 (2016) 371–392.
- [23] J. Xiong, R. Li, Y.Y. Lei, H. Chen, *J. Mater. Process. Technol.* 251 (2017) 12–19.
- [24] B.T. Wu, D.H. Ding, Z.X. Pan, D. Cuiuri, H.J. Li, J. Han, Z.Y. Fei, *J. Mater. Process. Technol.* 250 (2017) 304–312.
- [25] J.F. Wang, Q.J. Sun, H. Wang, J.P. Liu, J.C. Feng, *Mater. Sci. Eng. A* 676 (2016) 395–405.
- [26] Y. Ma, D. Cuiuri, C. Shen, H.J. Li, Z.X. Pan, *Addit. Manuf.* 8 (2015) 71–77.
- [27] H. Takagi, H. Sasahara, T. Abe, H. Sannomiya, S. Nishiyama, S. Ohta, K. Nakamura, *Addit. Manuf.* 24 (2018) 498–507.
- [28] G.H. Huang, D.D. Yin, J.W. Lu, H. Zhou, G.F. Quan, Q.D. Wang, *Mater. Sci. Eng. A* 720 (2018) 24–35.
- [29] C. Shen, Z.X. Pan, D. Cuiuri, D.H. Ding, H.J. Li, *Int. J. Adv. Manuf. Technol.* 88 (2017) 5–8.
- [30] S. Lee, H.J. Ham, S.Y. Kwon, S.W. Kim, C.M. Suh, *Int. J. Thermophys.* 34 (2013) 2343–2350.
- [31] M. Goodarzi, R. Choo, T. Takasu, J.M. Toguri, *J. Phys. D: Appl. Phys.* 31 (1998) 569–583.
- [32] E.R. Denlinger, J.C. Heigel, P. Michaleris, T.A. Palmer, *J. Mater. Process. Technol.* 215 (2015) 123–131.
- [33] T.A. Rodrigues, V. Duarte, J.A. Avila, G.S. Telmo, R.M. Mirandaa, J.P. Oliveira, *Addit. Manuf.* 27 (2019) 440–450.
- [34] Z.X. Pan, D.H. Ding, B.T. Wu, D. Cuiuri, H.J. Li, J. Norrish, *Trans. Intell. Weld. Manuf.* 1 (2018) 3–24.
- [35] A.A. Nayed-Hashemi, J.B. Clark, *Phase Diagrams of Binary Magnesium Alloys*, Monograph Series on Alloy Phase Diagrams, ASM International, 1988.
- [36] Y.Y. Guo, H.H. Pan, L.B. Ren, G.F. Quan, *Mater. Lett.* 247 (2019) 4–6.
- [37] L.B. Ren, G.F. Quan, M.Y. Zhou, Y.Y. Guo, Z.Z. Jiang, Q. Tang, *Mater. Sci. Eng. A* 690 (2017) 195–207.
- [38] Y. Zhu, X. Tian, J. Li, H. Wang, *J. Alloy. Compd.* 616 (2014) 468–474.